Theoretical perspective for internal quantum efficiency of thermally activated delayed fluorescence emitter in solid phase: A QM/MM study

Lili Lin [1], Jianzhong Fan [1], Chuan-Kui Wang[*]

Shandong Province Key Laboratory of Medical Physics and Image Processing Technology, School of Physics and Electronics, Shandong Normal University, 250014, Jinan, China

ARTICLE INFO

ABSTRACT

Excited state dynamics and charge transfer property of an orange-red thermally activated delayed fluorescence (TADF) emitter are theoretically investigated by a quantum mechanics/molecular mechanics (QM/MM) method and kinetic Monte Carlo simulation. The factors that influence internal quantum efficiency of the organic light-emitting diode (OLED) based on an asymmetric donor—acceptor (D—A) type molecule 10-(7-fluoro-2,3-diphenylquinoxalin-6-yl)-10H-phenoxazine (FDQPXZ) are analyzed. The results show that the intramolecular rotation of donor unit is restricted because of the enhanced intermolecular interaction in solid phase, which hinders the non-radiative consumption of the excited state energy. The decreased reorganization energy in solid phase is mainly contributed by dihedral angle in low-frequency (<500 cm^{-1}) region. Moreover, the non-radiative decay rate from the first singlet excited state (S1) to the ground state (S0) in solid phase is shown to be smaller than that in gas phase. In order to explore the charge transfer process in the film of FDQPXZ, Marcus theory is used to study the hole and electron transfer rates, and the charge mobility is thus obtained by Monte Carlo simulation. The theoretical calculation indicates that the FDQPXZ film is a *p*-type organic molecular material under the hopping mechanism. Intermolecular interaction for theoretical simulation of the working principle of OLEDs is highlighted.

1. Introduction

During the last two decades, organic light emitting diodes (OLEDs) have attracted considerable attention due to their promising application in flexible flat-panel displays and solid-state lighting sources [1—3]. Small OLED displays have been widely used in mobile phones such as Galaxy and OPPO. Although great progress has been made in the field of OLEDs, high external quantum yield of OLEDs remain a subject of great interest [4]. According to spin statistics, the singlet and triplet excitons are generated with the ratio of 1:3. For conventional fluorescent OLEDs, only singlet excitons can be used, all triplet excitons are wasted due to spin symmetry. In contrast, OLEDs use phosphorescent materials have achieved exciton utilization of 100% [5,6]. Owing to the rather

long lifetime of triplet excited states, a significant roll-off of the external efficiency has been observed with an increase of the current density [7]. Moreover, the phosphorescent materials are limited to Ir and Pt complexes, thus both fluorescence and phosphorescence OLEDs have advantages and disadvantages. Novel light emitting mechanisms are hoped and expected. Recently, Adachi's group proposes potential mechanism to achieve compatibility of harvesting both singlet and triplet excitons and avoiding triplet annihilation by the use of thermally activated delayed fluorescence (TADF) OLEDs [8—12]. For TADF-OLEDs, a small energy gap between lowest singlet (S1) and triplet (T1) excited state is regarded as the key factor for realizing high utilization of triplet excitons through a fast reverse intersystem crossing (RISC) process [13,14]. The general way to decrease the S1-T1 energy gap is connecting suitable donor (D) and acceptor (A) groups by a steric hindrance such as bulky, twist or spirojunction [15—17], because such methods can effectively decrease the spatial overlap between the highest occupied molecular orbital (HOMO) and lowest unoccupied molecular orbital (LUMO), furthermore, these configurations can modulate the

---

packing model in device through intermolecular interaction and change the charge transfer property which is related to the external quantum efficiency and efficiency roll-off of OLEDs [18,19]. Besides, the radiative and non-radiative decay processes from S1 to S0 as well as the intersystem crossing and reverse intersystem crossing processes between S1 and T1 play an important role in determining the internal quantum efficiency. Thus, investigations on excited state dynamics and charge transfer property for thermally activated delayed fluorescence emitter in device are crucial to understand the inner mechanism and further to design more efficient TADF-OLEDs.

In this work, an asymmetric donor—acceptor (D—A) type molecule 10-(7-fluoro-2,3-diphenylquinoxalin-6-yl)-10H-phenoxazine (FDQPXZ) is adopted to illustrate the excited state dynamics and charge transfer property for thermally activated delayed fluorescence emitter in solid phase. FDQPXZ is the first reported efficient orange-red TADF molecule, and it contains a fluorine-substituted quinoxaline as an electron-acceptor and phenoxazine (PXZ) as an electron-donor (shown in Fig. 1a) [19]. This work could serve as an important supplement to experiments in guiding the synthesis of more efficient orange and red TADF-OLEDs.

2. Computational details

For TADF molecules, the light-emitting efficiency is determined by the competition between the radiative decay rate and the non-radiative decay rate according to the following equations

$$\Phi_{PF} = \frac{K_r^S}{K_r^S + K_{nr}^S + K_{ISC}}. \tag{1}$$

$$\Phi_{ISC} = \frac{K_{ISC}}{K_r^S + K_{nr}^S + K_{ISC}}. \tag{2}$$

$$\Phi_{RISC} = \frac{K_{RISC}}{K_{RISC} + K_{nr}^T + K_r^T}. \tag{3}$$

where K_r^S and K_{nr}^S are the radiative and non-radiative decay rate from S1 to S0, K_{nr}^T is the non-radiative decay rate from T1 to S0, K_r^T is the phosphorescent rate, which can be neglected for organic molecules. K_{ISC} and K_{RISC} represents the intersystem crossing (ISC) and reverse intersystem crossing (RISC) rate between S1 and T1 respectively. Φ_{PF} is quantum efficiency of prompt fluorescence, Φ_{ISC} and Φ_{RISC} are the intersystem crossing efficiency and reverse intersystem crossing efficiency respectively [20]. Thus, theoretical calculations of radiative and non-radiative rate play an important role in predicting luminescent efficiencies. The radiative and non-radiative rate constants are evaluated by using the multimode coupled spectrum and rate theories, which are provided in detail in the supporting information (SI). For calculating the charge transfer rate, the Marcus theory is adopted. Corresponding details are shown in supporting information SII. The macroscopic charge mobility is obtained by subsequent Monte Carlo simulation [21].

Based on the X-ray crystal data of FDQPXZ, a computational quantum mechanics/molecular mechanics (QM/MM) method consisting of one central molecule for QM part and sixteen sounding molecules for the MM part is constructed by considering the effect of the environment (shown in Fig. 1b), and the detail packing structure is shown in Fig. 1c. Our QM/MM calculation is realized with the ONIOM method in *Gaussian 09* program [22]. Besides, the electronic embedding scheme is adopted in the ONIOM calculation. This model consists two "layers", the centered molecule is treated as a high layer and calculated by quantum mechanical method. The surrounding molecules are treated as low layer and computed by molecular mechanics with UFF forces field. As for the excited states (S1 and T1), the optimization of geometries and excitation energies calculation of the molecule are performed by the time-dependent density functional theory (TD-DFT) at BMK/6-31G(d) level. One should note that the "frozen optimization" is assumed in the optimization, which means that the surrounding molecules are frozen and only the centered molecule is optimized. To obtain the frequency of S0, S1 and T1, the calculations are performed by DFT and TD-DFT at the same computational levels of optimization.

In order to calculate the non-radiative rate and the charge mobility, the reorganization energy (details shown in Fig. 2) should be obtained first. E_{ab} and E_{em} is the absorption and emission energy. λ_{gs} and λ_{es} is the reorganization energy of the ground state S0 and the first excited state S1 respectively. The reorganization energy can be expressed as a summation of the contributions from normal modes (NM) relaxation as in the harmonic oscillator approximation

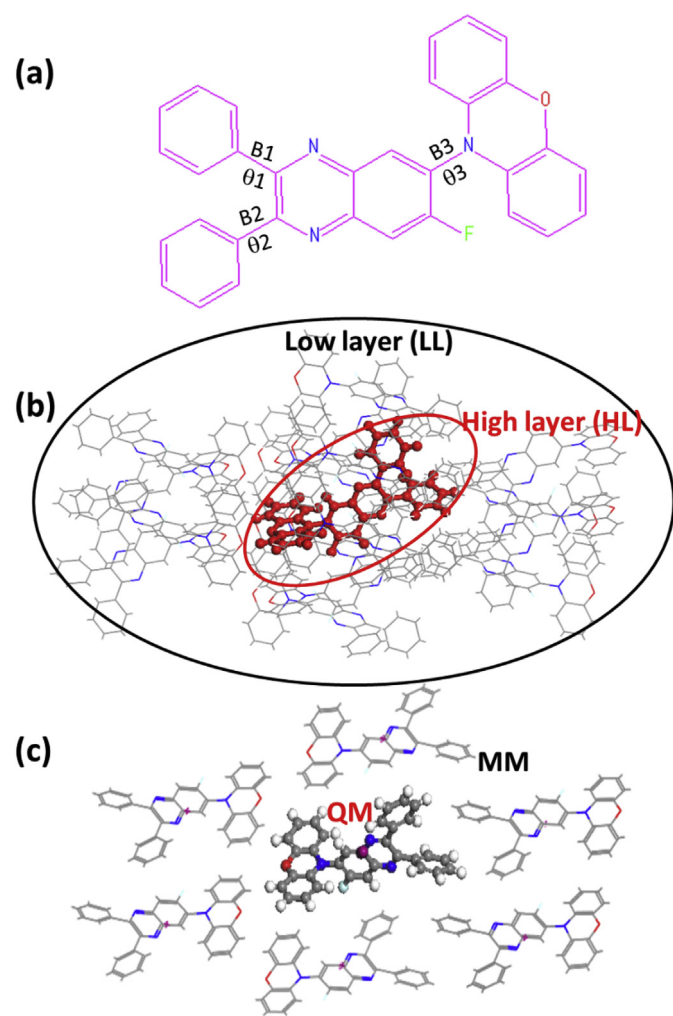$$\lambda_{gs} = \sum_{j \in gs} \lambda_j = \sum_{j \in gs} \hbar \omega_j S_j. \tag{4}$$

Fig. 1. (a) Chemical Structure of FDQPXZ. (b) ONIOM model: the centered molecule is treated as high layer and the surrounding molecules are fixed as low layer. (c) Close look at the packing structure.
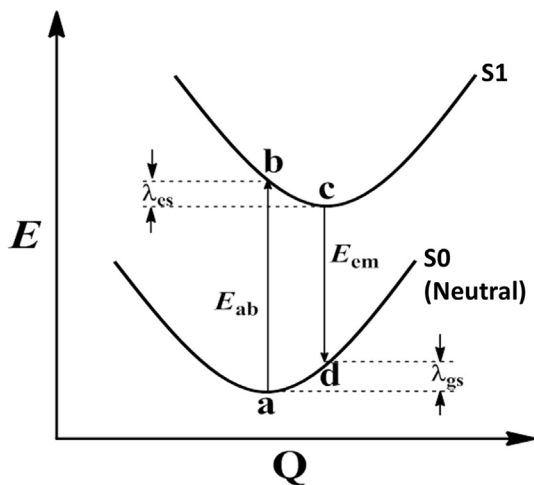
Fig. 2. Schematic representation of the adiabatic potential energy surfaces (PES) for S0 and S1 states.

$$\lambda_{es} = \sum_{j \in es} \lambda_j = \sum_{j \in es} \hbar\omega_j S_j. \tag{5}$$

$$S_j = \frac{\omega_j D_j^2}{2\hbar}. \tag{6}$$

here, D_j represents the displacement for the mode j between the equilibrium geometries of S0 and S1. As for the reorganization energy and NM analysis of anionic and cationic states, the above-mentioned method is also applicable. All these expectations can be realized in the DUSHIN program. Based on the calculation above, we calculate the non-radiative decay rate from S1 and T1 to S0 as well as the intersystem crossing rate and the reverse intersystem crossing rate between S1 and selected triplet states (T1, T2, T3) by using the multimode coupled thermal vibration correlation function (TVCF) formalism realized in MOMAP (Molecular Materials Property Prediction Package) which shows superiority in describing and predicting optical properties of polyatomic molecules [23–26].

Besides, in order to analyze the impact of molecular surroundings to electroluminescence properties of FDQPXZ, single molecule in gas phase is also studied with the same QM method as performed in the solid phase.

3. Results and discussion

Publications have shown that TD-DFT with nonhybrid functional always underestimates transition energies for charge transfer (CT) states due to the neglecting of long-range Columbic attraction between the separated electrons and holes. While time-dependent Hartree-Fork (TD-HF) usually suffers from the so-called electron correlation problem and it may overestimate transition energies. Thus, some ingenious approaches have been proposed and well applied recently, the optimal Hartree-Fock (OHF) method, LC-wPBE method and LC-BLYP method [27–29]. Here, we calculated the emission wavelength in gas and solid phase with different percentage of HF exchange incorporated within the functionals (HF %), all data are collected in Tables S1 and S2. Comparing with the experimental values (606 nm in neat film), BMK is determined and the following calculation is carried out with the BMK functional.

3.1. Influence of intermolecular interaction

To shed light on the influence of molecular surroundings to electroluminescence properties of FDQPXZ, selected geometry parameters (marked out in Fig. 1a) are listed in Table 1. Through analysis, we know B1 and B2 are weakly changed from gas phase to solid phase, and B3 possesses the maximum changes about 0.011 Å of T1 state from gas phase to solid phase. The calculated θ3 is 82.3° in S0 state which is consistent with the experimental result (81°). Moreover, a restricted dihedral angle change of θ3 can be seen when molecule transfers from gas phase to solid phase, for example, θ3 changes about 7.2° (from S0 to S1) and 42.7° (from S0 to T1) in gas phase, while these changes become 2.7° and 19.4° in solid phase. Thus an obviously restricted intramolecular rotation (RIR) can be seen which is caused by intermolecular interaction of neat film, and a small non-radiative decay rate can be expected in solid phase.

Moreover, the selected frontier molecular orbital distributions and orbital energies are shown in Fig. 3. As picture shows, HOMO is distributed on the donor part and LUMO is localized in the acceptor unit, and a typical D-A type feature can be found. Besides, intermolecular interactions almost have no effect on the distribution of HOMO and LUMO, but can increase the energy of HOMO greatly, thus a decreased HOMO-LUMO gap can be found in solid phase. Further, we calculated the UV-absorption and emission spectrums in toluene (Fig. 4a) and neat film (Fig. 4b). In toluene, the strong absorption peak at 317 nm (Exp: 334 nm) is attributed to the π-π* transition and the weak absorption at 444 nm (Exp: 400–500 nm) is assigned to the CT absorption from the donor to acceptor. An orange emission at 591 nm (Exp: 606 nm) of neat film can be seen, and the calculated phosphorescence wavelength is 624 nm (Exp: 616 nm in 77 K). All these data are in good agreement with the experimental results, and this can provide support for our adopted QM/MM method, ONIOM model and the selected BMK functional.

3.2. Huang-Rhys factor and reorganization energy

Huang-Rhys factor and reorganization energy are two effective ways to measure the non-radiative consumption of excited state energy. Schematic diagram is shown in Fig. 2 and corresponding data are collected in Table 2. We divide λ_{gs}, λ_{es} and λ_{all} into the contribution of bond length, bond angle and dihedral angle respectively, and detailed percentages are shown in Figs. S1 and S2. The contribution from bond length takes the major part for λ_{gs}, λ_{es} and λ_{all}, the total reorganization energy of FDQPXZ is 724.1 meV and 673.4 meV in gas and solid phase respectively, and the decreased energy (50.7 meV) is mainly contributed by changes of dihedral angle (39.7 meV) with the variation of bond length is 0.5 meV and bond angle is 10.5 meV. This is consistent with the result collected in Table 1, the rotation of dihedral angle is suppressed when molecule is in solid phase.

Further, we analyze the HR factor of each normal mode which is

Table 1
The selected bond lengths (B1, B2 and B3 (Å)) as well as dihedral angles (θ1, θ2 and θ3 (°)) marked in Fig. 1a for S0, S1 and T1 states in gas and solid phase respectively.

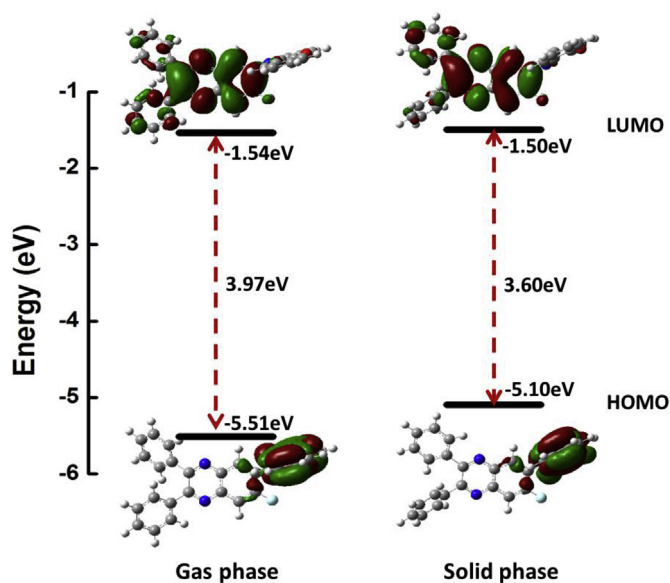| Geometry	Gas			Solid		
	S0	S1	T1	S0	S1	T1
θ1	143.8	142.6	142.0	155.5	153.1	160.3
θ2	143.9	149.1	154.5	123.4	120.5	127.4
θ3	82.3	89.5	125.2	91.0	93.7	71.6
B1	1.496	1.500	1.498	1.497	1.498	1.496
B2	1.496	1.492	1.481	1.496	1.496	1.489
B3	1.420	1.436	1.403	1.420	1.437	1.414

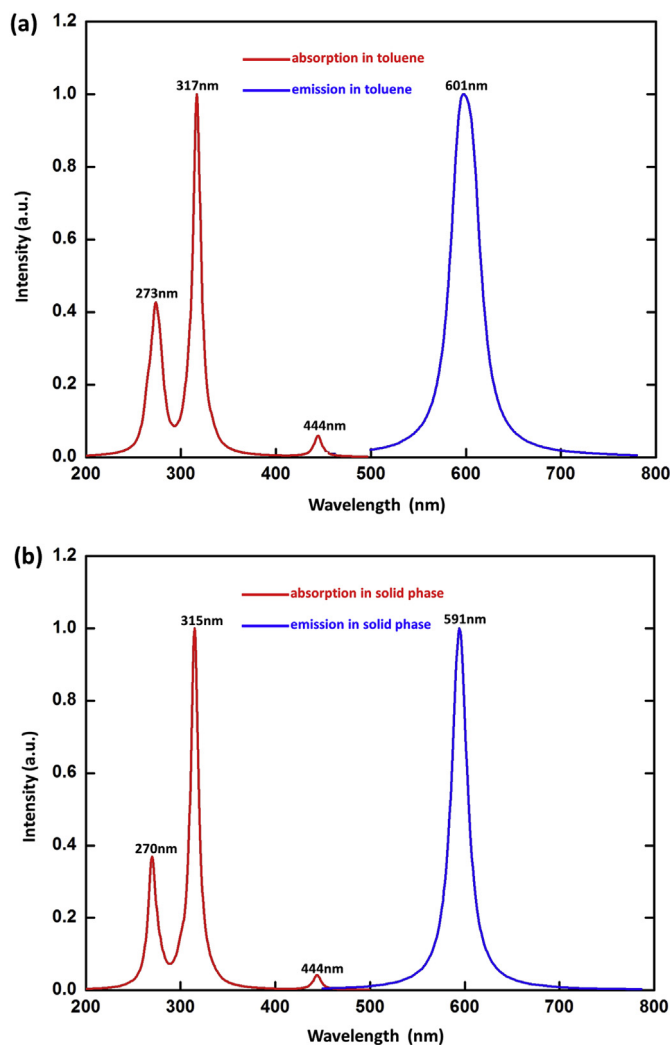**Fig. 3.** Frontier orbital distributions and their energy gaps of FDQPXZ in gas and solid phase respectively.

Fig. 4. The calculated absorption and emission spectrums for molecule in toluene (a) and in solid phase (b).

Table 2
Contributions to the reorganization energies (meV) from bond length, bond angle, and dihedral angle of FDQPXZ in the gas and solid phase.

	Gas			Solid		
	λ_{gs}	λ_{es}	λ_{all}	λ_{gs}	λ_{es}	λ_{all}
Bond length	246.3	250.7	497.0	248.8	247.7	496.5
Bond angle	46.6	49.2	95.8	40.4	44.9	85.3
Dihedral angle	39.3	92.0	131.3	21.1	70.5	91.6
Total	332.2	391.9	724.1	310.3	363.1	673.4

an important parameter in measuring the extent of the electron-vibration coupling shown in Fig. 5a and Fig. 5b. Comparing these HR factors, two distinct features can be found: (I) The maximum HR factor of FDQPXZ calculated in gas phase is about 2 times bigger than that in solid phase. (II) Vibration modes with large HR factor (>0.5) all appear in the low frequency region (<500 cm^{-1}) such as 24.0 cm^{-1} (HR = 3.49) and 28.8 cm^{-1} (HR = 1.57) in the gas phase, and no HR factor is larger than 1.4 in the solid state. Through analysis, we know the vibration modes especially these in low frequency regions are restricted, and these vibration modes with large HR factors in the gas phase are the out-of-plane twisting motion of PXZ which brings the change of the dihedral angle θ3 (show as insets in Fig. 5a and b). Besides, the reorganization energy (λ_{gs}) versus vibration mode both in gas phase and solid phase are shown in Fig. 5c and d. We find that (I) The λ_{gs} contributed by dihedral angle is 39.3 meV in gas phase whereas it decreases to 21.1 meV is solid phase (shown in Table 2), with the decreased energy is 18.2 meV (II) λ_{gs} in low frequency modes (<500 cm^{-1}) is decreased about 15.9 meV from gas phase to solid phase. This can confirm that, the intermolecular interaction in solid phase can restrict the low-frequency rotation of PXZ, and further brings decreased reorganization energies. Similar conditions can be acquired by analyzing λ_{es}, details are shown in Fig. S3. Due to the twisted molecular configuration of FDQPXZ, we neglect the intramolecular interaction such as intramolecular hydrogen-bonding and intramolecular π-π stacking interaction. More interests can refer to Tang's and Duan's work [30–32].

3.3. Excited state dynamics and quantum efficiency

In order to investigate the excited state dynamics, the energy landscape is necessary. Through TD-DFT calculations, the vertical excitation and adiabatic excitation energy diagrams are shown in Fig. 6. As we know, the vertical excitation energy can be used to measure the UV-absorption properties, and a precise adiabatic energy is needed to evaluate the emission properties. The calculated adiabatic energy gap between S1 and T1 is 0.06eV which is corresponding well with the 0.04eV measured by the fluorescence (298 K) and phosphorescence (77 K) spectrum experimentally. Thus, a fast reverse intersystem crossing process can be expected. Besides, the spin-orbit coupling constants (with the unit of cm^{-1}) between S1 and selected triplet states (T1, T2 and T3) calculated by *Dalton* package are listed in Table S3 [33]. It can be seen that the spin orbit coupling constants are all quite small both in gas phase and solid phase for organic molecule, so, a wise way to enhance the delayed fluorescence is decreasing the S1-T1 gap. According to the theory described in supporting information, the radiative and non-radiative decay rate as well as the ISC and RISC rate between selected singlet and triplet states are calculated and listed in Table 3. It is found that the non-radiative decay rate (K_{nr}^S) from S1 to S0 is 9.82×10^6 s^{-1} which is comparable with the radiative decay rate (K_r^S) and the ISC (K_{ISC}) rate, moreover, the calculated non-radiative decay rate in gas phase is 9.10×10^{10} s^{-1}. To confirm the
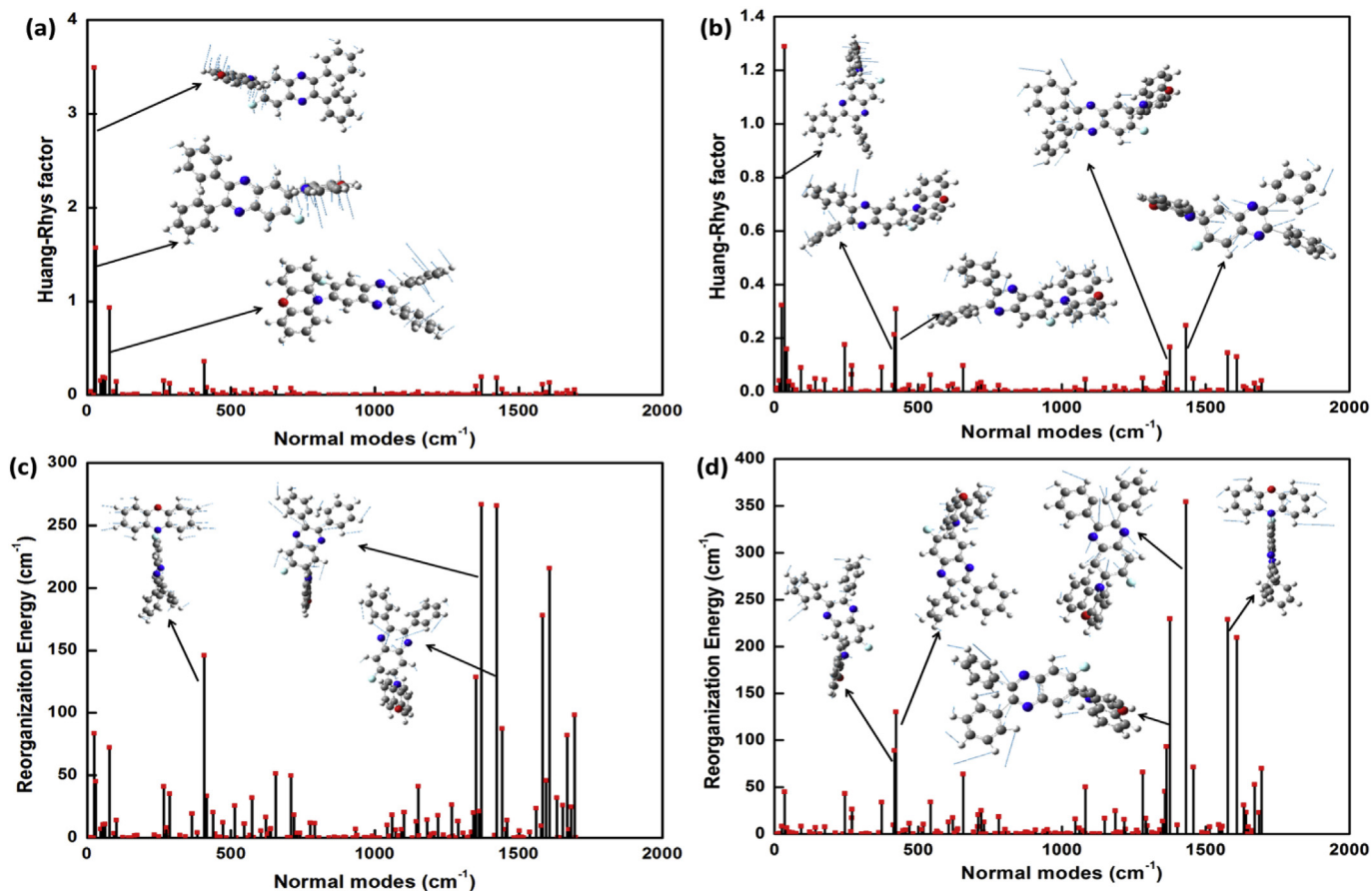
Fig. 5. The calculated HR factor of FDQPXZ in the gas phase (a) and solid state (b) as well as the reorganization energies in gas phase (c) and solid state (d). Selected vibration modes are shown as insets.
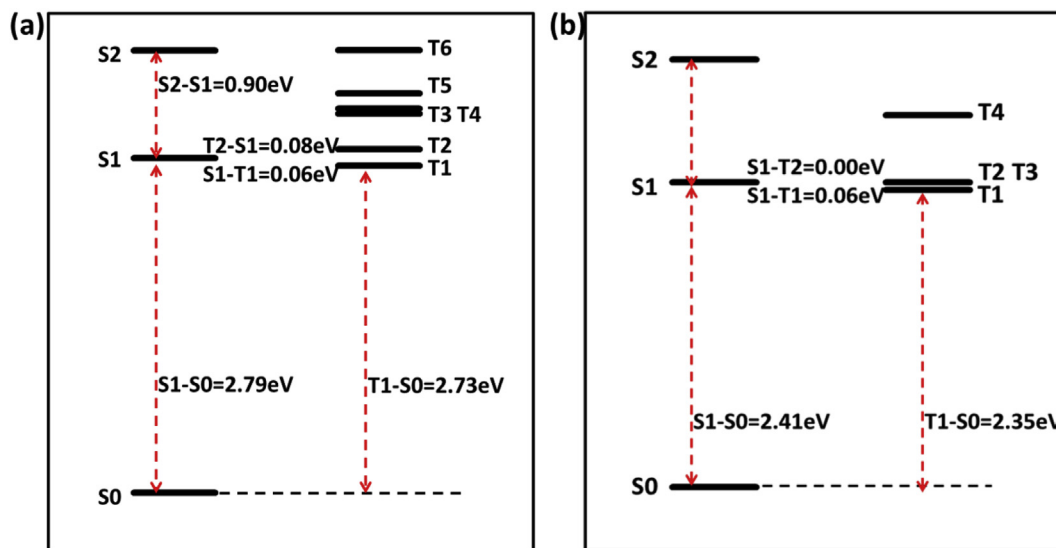

Fig. 6. The energy landscape of vertical excitation (a) and adiabatic excitation energy (b) for FDQPXZ in solid phase.

reliability of the internal conversion rate in our calculation, we plot the log K_{nr} (ΔE (eV)) parabola in Fig. 7. No vibrational feature is found in both two lines, which indicates the accuracy of the calculated K_{nr}. Thus, we know the intermolecular interactions can effectively hinder the non-radiative consumption of the excited

state energy. All these investigations demonstrate the importance of molecular interaction for theoretical simulating the working principle of OLEDs. Due to the quasi-degenerate triplet excited states and intermediate energy levels between S1 and T1, we define the effective ISC and RISC rate as

Table 3
The calculated rate constants of radiative and non-radiative as well as ISC and RISC of FDQPXZ in solid state.

|	$K_r^S(s^{-1})$ $(S1 \to S0)$	$K_r^T(s^{-1})$ $(T1 \to S0)$	$K_{nr}^S(s^{-1})$ $(S1 \to S0)$	$K_{nr}^T(s^{-1})$ $(T1 \to S0)$	K_{ISC} (s^{-1}) $(S1 \to T1)$	K_{RISC} (s^{-1}) $(T1 \to S1)$	K_{ISC} (s^{-1}) $(S1 \to T2)$	K_{RISC} (s^{-1}) $(T2 \to S1)$	K_{ISC} (s^{-1}) $(S1 \to T3)$	$K_{RISC}(s^{-1})$ $(T3 \to S1)$
Solid	9.22×10^5	1.20×10^{-1}	9.82×10^6	8.55×10^2	9.63×10^4	2.69×10^3	6.55×10^5	2.15×10^5	6.64×10^5	2.18×10^5
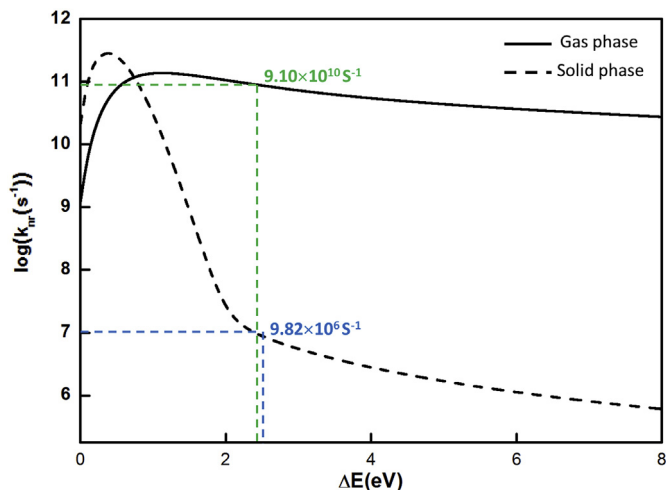
Fig. 7. Non-radiative decay rate K_{nr} versus the energy gap ΔE in gas and solid phase, the vertical line indicates the position of the adiabatic energy gap.

$$K_{ISC} = \frac{K_{S1-T1}^2 + K_{S1-T2}^2 + K_{S1-T3}^2}{K_{S1-T1} + K_{S1-T2} + K_{S1-T3}}. \quad (7)$$

$$K_{RISC} = \frac{K_{T1-S1}^2 + K_{T2-S1}^2 + K_{T3-S1}^2}{K_{T1-S1} + K_{T2-S1} + K_{T3-S1}}. \quad (8)$$

These effect rate constants for ISC and RISC are defined according to the distribution probability. Based on the formula above, we can obtain the effective ISC and RISC rate are $6.21 \times 10^5 \text{ s}^{-1}$ and $2.15 \times 10^5 \text{ s}^{-1}$ respectively in solid state. In addition, Penfold and Gibson et al. have demonstrated that the non-adiabatic coupling between the lowest local excitation triplet (^{3}LE) and lowest charge transfer triplet (^{3}CT) can open the possibility for second order coupling effect [34–39]. And this effect promotes ISC and RISC processes. In our manuscript, the ISC and RISC rates are calculated based on the Fermi's golden rule and first order perturbation theory (shown in SI), the second order coupling between these excited states with the same spin multiplicity is not considered in our calculation which is being actively pursued. Furthermore, combing the adiabatic energy landscape with the calculated radiative and non-radiative decay rates, the excited state dynamics for thermally activated delayed fluorescence molecule FDQPXZ is shown in Fig. 8. From Fig. 8, efficient hole and electron are injected from the anode and cathode respectively. The singlet and triplet excitons are generated with the ratio of 1:3, and 8.2% of singlet excitons are directly emitted as prompt fluorescence (PF) and 5.5% of them are transferred to triplet states through the ISC process, most of them (86.3%) are wasted non-radiatively. Under the electrical excitation in OLEDs, the theoretical maximum internal quantum efficiency (IQE) of the TADF-OLEDs can be estimated by following equations

$$\Phi_{DF} = \sum_{k=1}^{\infty} (\Phi_{ISC}\Phi_{RISC})^k \Phi_{PF} = \frac{\Phi_{ISC}\Phi_{RISC}}{1 - \Phi_{ISC}\Phi_{RISC}}\Phi_{PF}. \quad (9)$$
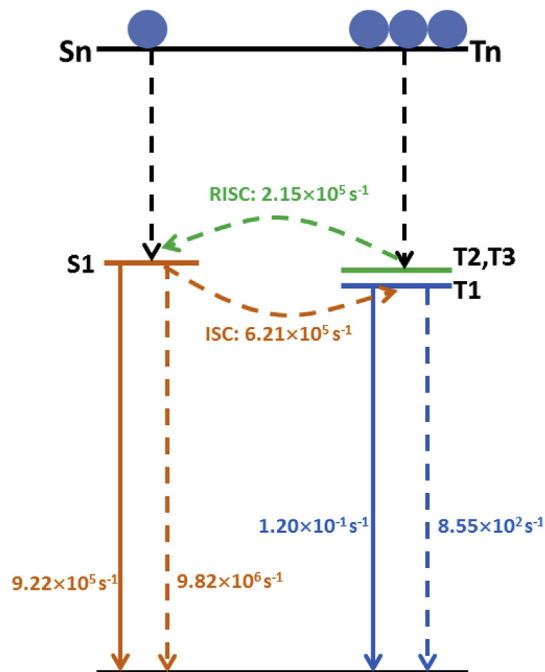
Fig. 8. Scheme of the electroluminescence process for FDQPXZ.

$$IQE = \gamma\eta_r\eta_{PL} = \gamma\left[0.25\Phi_{PF} + \frac{0.75 + 0.25(1 - \Phi_{PF})}{1 - \Phi_{PF}}\Phi_{DF}\right]. \quad (10)$$

where γ is the ration of charge combination to the electron and hole transportation. The calculated Φ_{PF} Φ_{ISC}, Φ_{RISC} and Φ_{DF} is 8.2%, 5.5%, 99.6% and 0.5% respectively, further, the IQE can be estimated to be 2.6%. However, the experimental result shows that the EQE can reach to 9% in device (CBP:PBD:FDQPXZ = 70:20:10, 40 nm). Difference between theoretical calculation and experimental measurement is caused by the large non-radiative decay process from S1 to S0. As a matter of fact, the OLED emitting layer is composed by host and guest molecules, the thermally activated delayed fluorescence molecules of FDQPXZ (guest) are made into device in the host-guest system. Here, we only calculated the photophysical properties in the neat film of guest. The packing mode of host-guest system can be obtained by performing molecular dynamics (MD) simulation, [40,41] which will be studied in advance. Furthermore, the importance of intermolecular interaction for theoretical simulation of the working principle of OLEDs is demonstrated.

3.4. Transfer integral and charge transfer rate

As illustrated in the previous chapter, the charge transport property is an important factor to determine the external quantum efficiency and efficiency roll-off of device. Good injection, bipolar and balanced hole and electron transfer in FDQPXZ neat film is expected to obtain successful TADF-OLEDs. Charge transfer properties are related to the charge reorganization energies. Moreover, molecular charge reorganization energy strongly depends on the

configuration differences between neutral and cationic (anionic) states. Thus, we calculate the reorganization energy by the normal mode analysis (NM) to determine the contribution of each vibration mode, and corresponding data are shown in Figs. S4 and S5. Through comparison, we know the total reorganization for cationic state (345.8 meV) is much smaller than that of anionic state (687.2 meV), and this indicates a restricted geometry change for cationic state. Further, a better hole transfer property of FDQPXZ can be expected than electron transfer and this prediction can be confirmed in the following chapter.

As illustrated in "*Computational details*" chapter, another important factor that can influence the transfer rate is the transfer integral. Based on the crystal structure, the charge transfer pathways are shown in Fig. 9, no obvious π-π stacking interaction can be found in the neat film and this can help to avoid the aggregation caused quenching (ACQ) effect, meanwhile a small charge transfer rate can be generated inevitably compared with the traditional *p*-type and *n*-type organic semiconductors. Representative transfer integral values are 16.3 meV, 6.9 meV and 1.9 meV with the electron transfer rate 6.7×10^9 s^{-1}, 1.2×10^9 s^{-1} and 9.3×10^7 s^{-1} respectively. Thus, for different packing model in crystal structure, the transfer integral largely depends on the relative positions of the two involved sites which can greatly change the transfer rate.

3.5. Hopping mechanism

Based on the abovementioned results, the kinetic Monte Carlo approach is adopted to simulate the hole and electron transfer process in organic single crystal systems. The squared displacement versus the transfer time is shown in Fig. 10. Although, the individual displacement is disordered, a quite liner relationship can be found
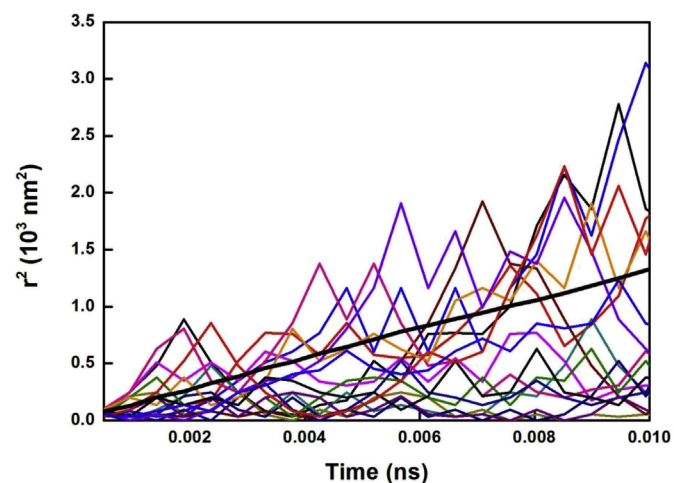

Fig. 10. Hole transport trajectories versus time. The straight line (black) is the average values of the square displacements versus time.

between the average values of all trajectories with the time. Based on the Einstein equation, the calculated average mobility is 0.13 cm^2/V and 0.63×10^{-3} cm^2/V for hole and electron respectively at 298 K. Thus, we know, the FDQPXZ neat film is a hole transfer material and this is due to the molecular component PXZ who possesses a good hole transfer ability and often be used an efficient electron donor part. Besides, the temperature dependence of the charge mobility is an important property for organic molecular materials. The calculated hole and electron mobility increases with the improvement of the temperature (show in Fig. 11), and the calculated reorganization energies of hole (345 meV) and electron (687 meV) are all larger than hole (24 meV) and electron (16 meV) transfer integral. All these features ($\frac{du}{dT} > 0$, $\lambda \gg V$) indicate a hopping mechanism for FDQPXZ neat film. So, the FDQPXZ is *p*-type material and possesses the hopping model feature.

4. Conclusion

In summary, we investigate the excited state dynamics and hole-electron transfer properties through the QM/MM method and kinetic Monte Carlo simulation for the FDQPXZ film. Results show that the rotation of donor can be efficiently restricted by enhanced
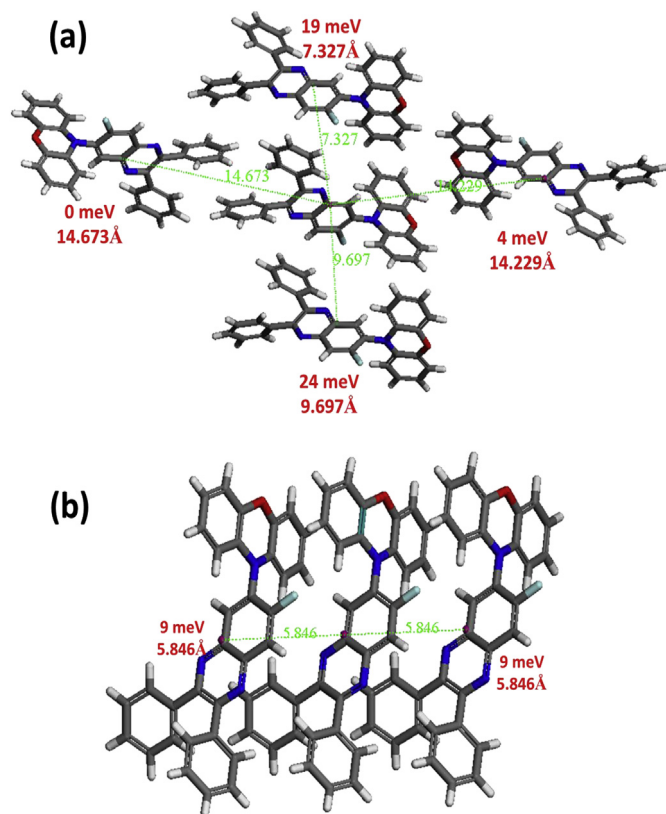

Fig. 9. Hole transfer pathways with transfer integral and distance for neat film of FDQPXZ. (a) X-axis view, (b) Y-axis view.
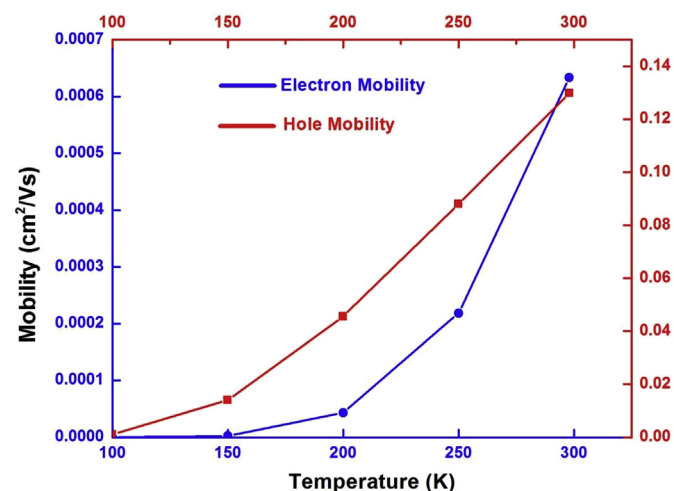

Fig. 11. Temperature dependence of the mobility of FDQPXZ (neat film).

intermolecular interaction in solid phase, this brings a decreased non-radiative decay rate and the non-radiative consumption ways of the excited state energy are hindered. Furthermore, through comparing the reorganization energy in gas phase (724.1 meV) and in solid phase (673.4 meV), we know the decreased reorganization energy (50.7 meV) is mainly contributed by dihedral angle (39.7 meV) which is associated with the rotation of donor part in low-frequency (<500 cm^{-1}) region. Furthermore, the hole and electron transfer rates of FDQPXZ film are studied by Marcus theory and the charge mobility is thus obtained through Monte Carlo simulation. Results show that the film is a p-type material under the hopping mechanism. Thus, the internal quantum efficiency and charge mobility are investigated for orange-red organic light emitting materials, and the importance of molecular interaction for theoretical simulation of the working principle of OLEDs is highlighted. Moreover, the method adopted in this article not only can provide a reasonable simulation for the emitting layers in OLEDs but also can be used to reveal the aggregation-induced emission (AIE) and aggregation-caused quenching (ACQ) phenomenon, and corresponding studies are in process.

Conflicts of interest

There are no conflicts of interest to declare.

Acknowledgments

Appendix A. Supplementary data

Supplementary data related to this article can be found at https://doi.org/10.1016/j.orgel.2017.09.021.

References

[1] C.W. Tang, S.A. VanSlyke, Appl. Phys. Lett. 51 (1987) 913.
[2] J.H. Jou, S. Kumar, A. Agrawal, T.H. Li, S. Sahoo, J. Mater. Chem. C 3 (2015), 2974.
[3] K. Yoshida, T. Matsushima, H. Nakanotani, C. Adachi, Org. Electron. 31 (2016) 191.
[4] B.S. Nehls, S. Füldner, E. Preis, T. Farrell, U. Scherf, Macromolecules 38 (2005) 687.
[5] C. Adachi, M.A. Baldo, M.E. Thompson, S.R. Forrest, J. Appl. Phys. 90 (2001), 5048.
[6] L. Xiao, S.-J. Su, Y. Agata, H. Lan, J. Kido, Adv. Mater 21 (2009) 1271.
[7] S. Reineke, K. Walzer, K. Leo, Phys. Rev. B 75 (2007), 125328.
[8] H. Uoyama, K. Goushi, K. Shizu, H. Nomura, C. Adachi, Nature 492 (2012) 234.
[9] S. Wu, M. Aonuma, Q. Zhang, S. Huang, T. Nakagawa, K. Kuwabara, C. Adachi, J. Mater. Chem. C 2 (2014) 421.
[10] K. Shizu, H. Noda, H. Tanaka, M. Taneda, M. Uejima, T. Sato, K. Tanaka, H. Kaji, C. Adachi, J. Phys. Chem. C 119 (2015), 26283.
[11] A.S.D. Sandanayaka, T. Matsushima, C. Adachi, J. Phys. Chem. C 119 (2015), 23845.
[12] P.L. Santos, J.S. Ward, P. Data, A.S. Batsanov, M.R. Bryce, F.B. Dias, A.P. Monkman, J. Mater. Chem. C 4 (2016), 3815.
[13] T. Sato, M. Uejima, K. Tanaka, H. Kaji, C. Adachi, J. Mater. Chem. C 3 (2015) 870.
[14] Q. Zhang, H. Kuwabara, W.J. Potscavage, S. Huang, Y. Hatae, T. Shibata, C. Adachi, J. Am. Chem. Soc. 136 (2014), 18070.
[15] T. Nakagawa, S.Y. Ku, K.T. Wong, C. Adachi, Chem. Commun. 48 (2012), 9580.
[16] G. Méhes, H. Nomura, Q. Zhang, T. Nakagawa, C. Adachi, Angew. Chem. Int. Ed. 51 (2012), 11311.
[17] K. Nasu, T. Nakagawa, H. Nomura, C.J. Lin, C.H. Cheng, M.R. Tseng, T. Yasuda, C. Adachi, Chem. Commun. 49 (2013), 10385.
[18] L. Lin, H. Geng, Z. Shuai, Y. Luo, Org. Electron. 13 (2012), 2763.
[19] L. Yu, Z. Wu, G. Xie, C. Zhong, Z. Zhu, H. Cong, D. Ma, C. Yang, Chem. Commun. 52 (2016), 11012.
[20] Y. Tao, K. Yuan, T. Chen, P. Xu, H. Li, R. Chen, C. Zheng, L. Zhang, W. Huang, Adv. Mater 26 (2014), 7931.
[21] L. Wang, Q. Li, Z. Shuai, L. Chen, Q. Shi, Phys. Chem. Chem. Phys. 12 (2010), 3309.
[22] M.J. Frisch, G.W. Trucks, H.B. Schlegel, G.E. Scuseria, M.A. Robb, J.R. Cheeseman, G. Scalmani, V. Barone, B. Mennucci, G.A. Petersson, H. Nakatsuji, M. Caricato, X. Li, H.P. Hratchian, A.F. Izmaylov, J. Bloino, G. Zheng, J.L. Sonnenberg, M. Hada, M. Ehara, K. Toyota, R. Fukuda, J. Hasegawa, M. Ishida, T. Nakajima, Y. Honda, O. Kitao, H. Nakai, T. Vreven, J.A. Montgomery Jr., J.E. Peralta, F. Ogliaro, M. Bearpark, J.J. Heyd, E. Brothers, K.N. Kudin, V.N. Staroverov, R. Kobayashi, J. Normand, K. Raghavachari, A. Rendell, J.C. Burant, S.S. Iyengar, J. Tomasi, M. Cossi, N. Rega, J.M. Millam, M. Klene, J.E. Knox, J.B. Cross, V. Bakken, C. Adamo, J. Jaramillo, R. Gomperts, R.E. Stratmann, O. Yazyev, A.J. Austin, R. Cammi, C. Pomelli, J.W. Ochterski, R.L. Martin, K. Morokuma, V.G. Zakrzewski, G.A. Voth, P. Salvador, J.J. Dannenberg, S. Dapprich, A.D. Daniels, O. Farkas, J.B. Foresman, J.V. Ortiz, J. Cioslowski, D.J. Fox, Gaussian09 Revision A.01, Gaussian Inc., Wallingford CT, 2009.
[23] Y. Niu, Q. Peng, C. Deng, X. Gao, Z. Shuai, J. Phys. Chem. A 114 (2010), 7817.
[24] Q. Peng, Q. Shi, Y. Niu, Y. Yi, S. Sun, W. Li, Z. Shuai, J. Mater. Chem. C 4 (2016), 6829.
[25] H. Ma, W. Shi, J. Ren, W. Li, Q. Peng, Z. Shuai, J. Phys. Chem. Lett. 7 (2016), 2893.
[26] Y. Niu, Q. Peng, Z. Shuai, Sci. China Ser. B 51 (2008), 1153.
[27] S. Huang, Q. Zhang, Y. Shiota, T. Nakagawa, K. Kuwabara, K. Yoshizawa, C. Adachi, J. Chem. Theory. Comput. 9 (2013), 3872.
[28] H. Sun, C. Zhong, J.L. Bredas, J. Chem. Theory. Comput. 11 (2015), 3851.
[29] T.J. Penfold, J. Phys. Chem. C 119 (2015), 13535.
[30] Y. Watanabe, H. Sasabe, D. Yokoyama, T. Beppu, H. Katagiri, J. Kido, J. Mater. Chem. C 4 (2016), 3699.
[31] Y. Zhang, D. Zhang, M. Cai, Y. Li, D. Zhang, Y. Qiu, L. Duan, Nanotechnology 27 (2016), 094001.
[32] Q. Zhu, Y. Zhang, H. Nie, Z. Zhao, S. Liu, K.S. Wong, B.Z. Tang, Chem. Sci. 6 (2015), 4690.
[33] Dalton, a Molecular Electronic Structure Program, http://daltonprogram.org.
[34] J. Gibson, A.P. Monkman, T.J. Penfold, ChemPhysChem 17 (2016), 2956.
[35] J. Gibson, T. Penfold, Phys. Chem. Chem. Phys. 19 (2017), 8428.
[36] M.K. Etherington, J. Gibson, H.F. Higginbotham, T.J. Penfold, A.P. Monkman, Nat. Commun. 7 (2016).
[37] X.-K. Chen, S.-F. Zhang, J.-X. Fan, A.-M. Ren, J. Phys. Chem. C 119 (2015), 9728.
[38] Q. Peng, Y. Niu, Q. Shi, X. Gao, Z. Shuai, J. Chem. Theory. Comput. 9 (2013), 1132.
[39] R. Huang, J. Avo, T. Northey, E. Chaning-Pearce, P.L. dos Santos, J.S. Ward, P. Data, M.K. Etherington, M.A. Fox, T.J. Penfold, M.N. Berberan-Santos, J.C. Lima, M.R. Bryce, F.B. Dias, J. Mater. Chem. C 5 (2017) 6269.
[40] T. Zhu, T. Van Voorhis, J. Phys. Chem. C 120 (2016), 19987.
[41] X. Zheng, Q. Peng, L. Zhu, Y. Xie, X. Huang, Z. Shuai, Nanoscale 8 (2016), 15173.